2010

High Efficiency Development of a Rotary Compressor by Clarification of its Shaft Dynamic Motion

Yoko Kitsunai
Panasonic Corporation Living Environment Development Center

Masaru Matsui
Panasonic Corporation Living Environment Development Center

Shingo Oyagi
Panasonic Corporation Home Appliances Company Corporate Engineering Division Appliances Development Center

High Efficiency Development of a Rotary Compressor by Clarification of its Shaft Dynamic Motion

Yoko KITSUNAI[1]*, Masaru MATSUI[2], Singo OYAGI [2]

[1] Living Environment Development Center, Panasonic Corporation,
3-1-1 Yagumo-naka-machi, Moriguchi City, Osaka, 570-8501, Japan
Phone:+81-6-6906-4846, Fax:+81-6-6904-5163, E-mail:kitsunai.yoko@jp.panasonic.com

[2] Appliances Development Center, Panasonic Corporation,
2-3-1-2 Noji-higashi, Kusatsu City, Shiga 525-8555, Japan
Phone:+81-77-561-5664, Fax:+81-77-563-1967, E-mail:matsui.masaru@jp.panasonic.com

* Corresponding Author

ABSTRACT

In this study, an elasto-hydrodynamic-lubrication analysis was developed to clarify a shaft dynamic motion of a rotary compressor. Based on the analysis, a shaft supporting mechanism in the upper bearing was shown and it was found that to form an anural depression on the shaft surface affects both the reduction of losses and increase in performance of the rotary compressor. As a result, experimental results showed increase in coefficient of performance (COP) by 0.6 %.

1. INTRODUCTION

Due to recent environmental problems represented by global warming, a demand for more efficient electric household appliances such as air conditioning systems, which occupy the highest percentage of 25.1 % among residential electric energy consumption in Japan, has been increasing. Thus, an attempt was made to improve an efficiency of a rotary compressor that is a main component of an air conditioning system. To clarify the shaft dynamic motion during the operation, which affects the compressor efficiency and performance greatly, an elasto-hydrodynamic-lubrication taking an elastic deformation of both the bearing and shaft into consideration was developed. In this study, a description of the analysis and a development for increase in the efficiency of the compressor using the analysis was presented.

2. ANALYSIS METHOD

2.1 Outline

Figure 1 shows the image of the shaft of our rotary compressor during its operation. In this figure, x axis, y axis, z axis and θ represent a vane installation direction, direction rotated by 90 degree from x axis toward the shaft rotation, shaft height direction and shaft rotation angle, respectively (Figure 1). As shown in Figure 1, a load acting on a crank pin due to refrigerant pressure difference, centrifugal forces produced by the shaft itself and other attached parts such as upper and lower balance weights and a magnetic attractive force generated between the rotor and stator act on the rotary compressor shaft during the operation. The shaft, on which these forces act, is supported by support forces of the bearing formed by two factors, i.e., lubricant oil film pressure p generated between the shat and bearing due to a change in oil film thickness h, and solid contact pressure p_c generated by solid contact between the shaft outer surface and bearing inner surface.

At a rotation angle, the shaft is supposed to deform due to above-mentioned forces, i.e., the load acting on the crank pin, centrifugal forces, magnetic attractive force and support forces, and take a posture which meets the balance of force and moment. This analysis solves the shaft posture including both the shaft and bearing deformation at each

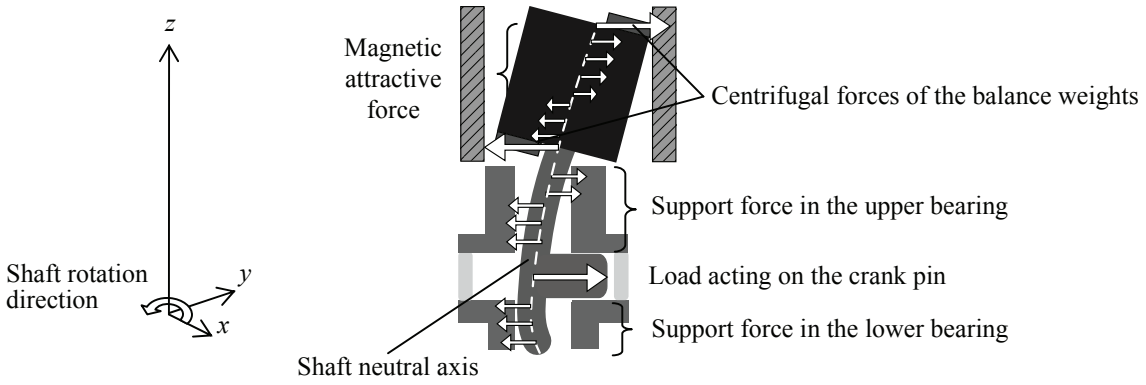

(a) Vertical view

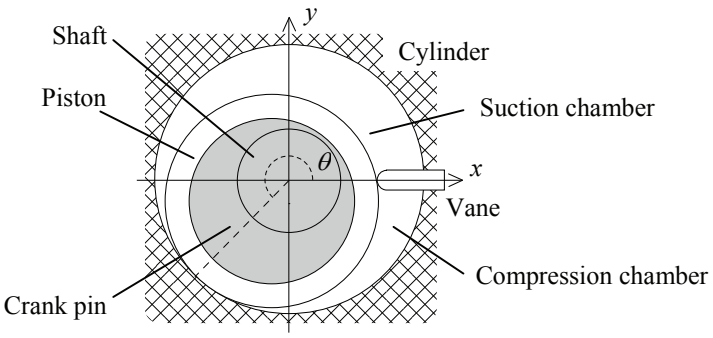

(b) Cross sectional view

Figure 1: Image of the rotary compressor shaft

rotation angle. Based on the resultant posture, the distribution of the oil film thickness h, oil film pressure p and solid contact pressure p_c can be obtained. A locus of the shaft neutral axis during the shaft rotation can be also obtained. Using these data, a shaft supporting mechanism and effects of the shaft deformation on a refrigerant gas leakage can be investigated.

Figure 2 shows the calculation flow at a rotation angle. First, support forces Fb_x^*, Fb_y^* are assumed and the shaft deformation is calculated by the assumed support forces Fb_x^*, Fb_y^*. Then, the oil film thickness h between the shaft and bearing was calculated by obtained deformation values. Based on h, the oil film pressure p and solid contact pressure p_c can be calculated and the support forces Fb_x, Fb_y are obtained. When the support forces Fb_x, Fb_y and previously-assumed support forces Fb_x^*, Fb_y^* have same values, the shaft posture is determined at the rotation angle.

2.2 Support force of the bearing

A modified Reynolds equation analysis taking an effect of surface roughness in consideration (Patir and Cheng, 1978 and Patir and Cheng, 1979) is applied for hydrodynamic lubrication analysis (HL analysis) to calculate the oil film pressure p.

$$\frac{\partial}{r\partial\theta}\left(\phi_x \frac{h^3}{12\eta}\frac{\partial p}{r\partial\theta}\right)+\frac{\partial}{\partial z}\left(\phi_z \frac{h^3}{12\eta}\frac{\partial p}{\partial z}\right)=\frac{U}{2}\left(\frac{\partial \bar{h}_T}{r\partial\theta}+\sigma\frac{\partial \phi_s}{r\partial\theta}\right)+\frac{\partial \bar{h}_T}{\partial t} \tag{1}$$

where p, r, θ, h, $\bar{h}_T$, η, U and ϕx, ϕz, ϕs are the oil film pressure, radius of the shaft, shaft rotation angle, oil film thickness at a local point, expectation of h, lubricant oil viscosity, shaft rotation speed and collection factors, respectively.

A solid contact theory by Greenwood (Greenwood and Tripp, 1970 and Patir and Cheng, 1978) is applied for contact pressure analysis (CP analysis) to calculate the solid contact pressure p_c.

$$p_c = 4.4086 \times 10^{-5} \cdot k' \cdot E' \cdot \left(4.0 - \frac{h}{\sigma}\right)^{6.804} \quad (h < 4\sigma) \tag{2}$$

where p_c, k', E' and σ are the solid contact pressure, factor of material and surface property of the two contact objects, combined young's modulus of the shaft and bearing and combined surface roughness of the shaft and bearing, respectively.
The support forces Fb_x, Fb_y are calculated by integrating p and p_c obtained from Equation (1) and (2) on whole bearing surface (Support force calculation: SF calculation).

2.3 Bearing deformation

The bearing deformation is induced by the oil film pressure p and solid contact pressure p_c generated between the shaft and bearing. To analyze the deformation, bearing structure is subdivided into cubic elements and 3-dimensional finite element method (FEM) is applied (Bearing deformation analysis: BD analysis).

$$[K_B][\delta_B] = [F_B] \tag{3}$$

In Equation (3), $[F_B]$ is the nodal forces acting on each node existing on the bearing inner surface, which are calculated from the oil film pressure p and solid contact pressure p_c. $[\delta_B]$ is the nodal displacements of the bearing elements. $[K_B]$ is the global stiffness matrix of the bearing

2.4 Shaft deformation

As shown in Figure 1, it can be assumed that only x-directional and y-directional forces act on the shaft. And the shaft is long enough to apply a pure bending theory, in which x-directional forces induce only x-directional deformation and y-directional forces induce only y-directional deformation. Therefore, to analyze the shaft deformation, the shaft structure is subdivided into line elements along z axis and 1-dimensional FEM is applied (Shaft deformation analysis: SD analysis).

$$[K_S][\delta_S] = [F_{S1}] + [F_{S2}] + [F_{S3}] + [F_{S4}] \tag{4}$$

where $[K_S]$, $[\delta_S]$, $[F_{S1}]$, $[F_{S2}]$, $[F_{S3}]$ and $[F_{S4}]$ are the global stiffness matrix of the shaft, nodal displacements of the shaft elements, load acting on the crank pin, support forces, centrifugal forces produced by the shaft itself and other attached parts and magnetic attractive force of the motor, respectively. The load acting on the crank pin $[F_{S1}]$ is given as an initial data. The magnetic attractive force $[F_{S4}]$ is given as follows; first, a distribution of an air gap that is a clearance between the rotor and stator is calculated by using obtained displacement values of some nodes, which represent the rotor. Then, based on previously-measured relationship between the air gap and magnetic attractive force, $[F_{S4}]$ can be given.
The shaft during the operation has no constrained node. Without it, Equation (4) becomes indefinite

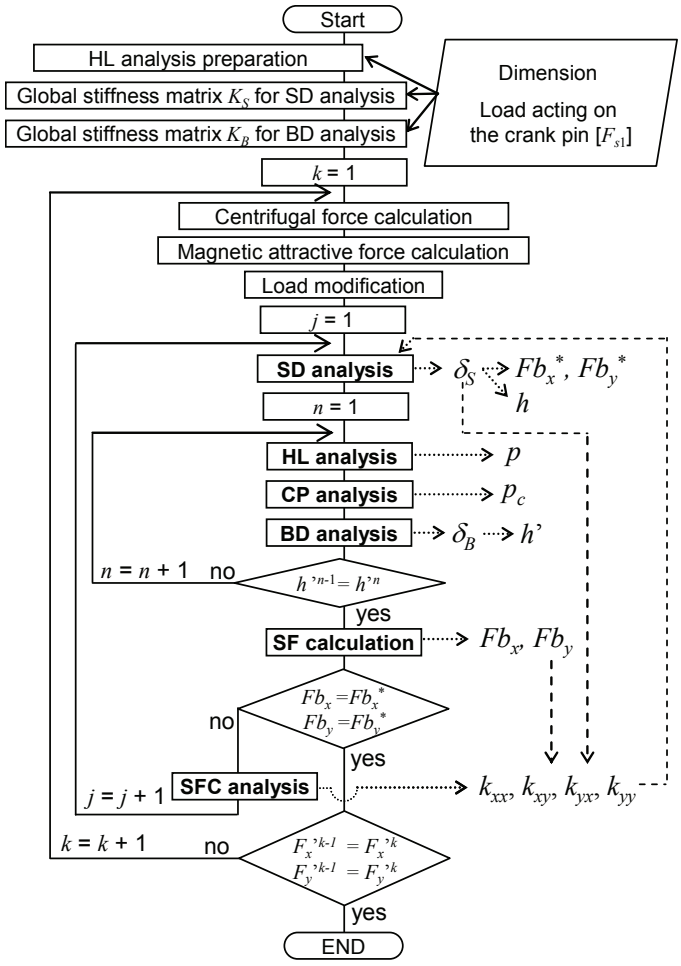

Figure 2: Calculation flow

and can not be calculated. To solve the issue, support force constants k_{xx}, k_{xy}, k_{yx}, k_{yy}, which represent relationships between a variation of shaft deformations and variation of support forces, are introduced. k_{xx} represents the relationship between x-directional variation of the shaft deformation and x-directional variation of the support force. k_{xy} represents the relationship between x-directional variation of the shaft deformation and y-directional variation of the support force. k_{yx} represents the relationship between y-directional variation of the shaft deformation and x-directional variation of the support force. k_{yy} represents the relationship between y-directional variation of the shaft deformation and y-directional variation of the support force. By applying the model of spring system in Equation (4), i.e., $[F_{S2}]$ is represented with the support force constants k_{xx}, k_{xy}, k_{yx}, k_{yy} and unknown factor $[\delta_S]$, Equation (4) can be solved and the nodal displacement of the shaft elements $[\delta_S]$ can be obtained.
When a support force constant is assumed, assumed support forces Fb_x^*, Fb_y^* are set and the shaft deformation (the shaft nodal displacement) can be obtained. Based on the obtained deformation value, a distribution of the oil film thickness h is calculated, and then, support forces Fb_x, Fb_y is obtained from HL analysis, CP analysis and BR calculation. The assumed support force constant should be modified so that the resultant support forces Fb_x, Fb_y have same value as previously assumed support forces Fb_x^*, Fb_y^*. Support force constants are repeatedly modified by little by little (Support force constant analysis: SFC analysis) until the resultant and assumed values become same.

3. RESULTS AND DISCUSSION

3.1 The shaft supporting mechanism in the upper bearing

The analysis was examined under two operating conditions. One is heating half-capacity operation, which is most frequently-used operating condition in Japan. The shaft rotating speed under this condition is 26 Hz. Another is high rotating operation. The shaft rotating speed is 130 Hz. This operation can be used for rapid heating to meet recent high market needs.
Figure 3 shows the shaft dynamic motion under heating half-capacity operation. In Figure 3, x axis, y axis, z axis and θ represent a vane installation direction, direction rotated by 90 degree from x axis toward the shaft rotation, shaft height direction and shaft rotation angle, respectively. Values of x and y axis are normalized by an average clearance between the shaft and bearing. Values of z axis are normalized by the shaft length. As shown in Figure 3, it was found that the shaft is bending and tilting during the rotation.
Figure 4 shows a comparison of the shaft deformation between half-capacity operation (26 Hz) and high rotating operation (130 Hz). The shaft deformations shown in this figure were obtained at the rotation angle where the maximum shaft deformation was obtained in Figure 3 (θ = 300°). As shown in Figure 4, the shaft deformation differs according on the operating condition. The shaft deformation under high rotating operation was 8 times bigger than that under half-capacity operation. This phenomenon is thought to be caused by the centrifugal forces, which is

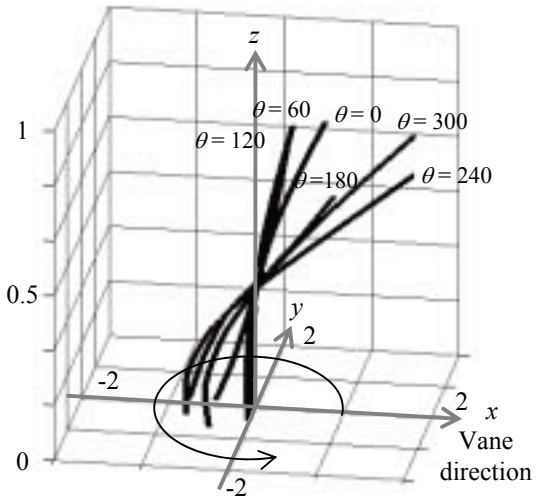

Figure 3: Shaft dynamic motions under heating half-capacity operation (26 Hz)

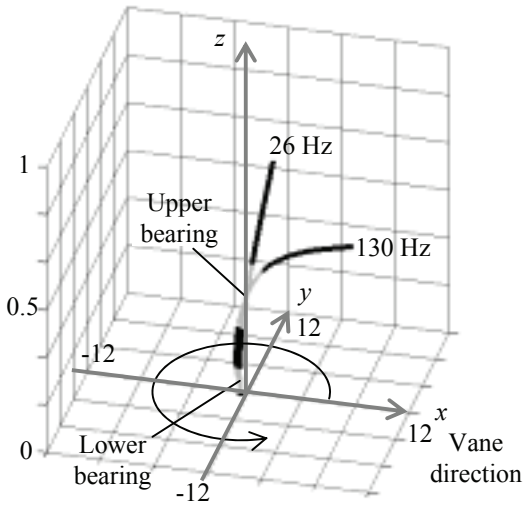

Figure 4: Shaft deformation under heating half-capacity operation (26 Hz) and high rotating operation (130 Hz)

affected by the square of the rotating speed. Due to 5-times-bigger shaft rotating speed, the centrifugal forces produced by the upper and lower balance weights under high rotating operation is 25 times bigger than that under half-capacity operation. Therefore, 25-times-bigger forces induced the greater shaft deformation.

To investigate the distribution of the oil film pressure p and solid contact pressure p_c generated at the rotation angle shown in Figure 4, the summations of p and p_c ($p + p_c$) were detected at 6 points along z-axial direction, i.e., bottom, middle and top of the upper and lower bearing. Then, pressure maximums, which are maximum values of each summation ($p + p_c$) among the corresponding circumferential direction, were obtained. These pressure maximum were normalized by a surrounding pressure and are shown in Table 1. In Table 1, (a) and (b) show the pressure maximum obtained under half-capacity operation (26 Hz) and high rotating operation (130 Hz), respectively. As shown in Table 1, the tendency of the change in the pressure maximum differs according to the operating condition. This difference indicates that the shaft supporting mechanism in the bearing differs between half-capacity operation and high rotating operation.

The contribution to the shaft supporting of the upper bearing is supposed to be smaller than that of the lower bearing under heating half-capacity operation. This is because the pressure maximums obtained at the lower bearing were around 3 times as big as the surrounding pressure although the pressure maximums obtained at the upper bearing were only 1.2-1.4 times bigger than the surrounding pressure (Table 1(a)). Based on this result, it is suggested that the upper bearing can be reduced. The reduction of the upper bearing possibly reduces the friction losses of the upper bearing and improves the efficiency.

As same as heating half-capacity operation, under high rotating operation, the contribution to the shaft supporting of the middle of the upper bearing is supposed to be smallest among the other parts because the pressure maximum obtained there was the smallest and it was only 1.7 times bigger than the surrounding pressure (Table 1(b)).

As shown in the top line of Table 1(a) and (b), however, the pressure maximum obtained at the top of the upper bearing under high rotating operation was the largest and it was 7 times bigger than the surrounding pressure although that under heating half-capacity operation was the smallest and it was only 1.2 times bigger than the surrounding pressure. Based on this result, it was found that the top of the upper bearing, which hardly contributes the shaft supporting under the heating half-capacity operation, contributes the most to the shaft supporting under the high rotating operation.

Therefore, it was suggested that the reduction of the middle of the upper bearing has a possibility to reduce the friction losses without large reduction of the shaft supporting capacity. Based on this, an attempt was made to form an annular depression on the shaft surface at the middle of the upper bearing.

Table 1: Pressure maximum normalized by the surrounding pressure

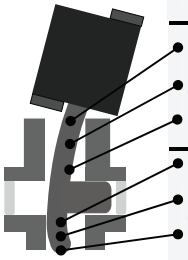

		(a)Heating half-capacity operation	(b) High rotating operation
Upper bearing	Top	1.21	7.07
	Middle	1.34	1.68
	Bottom	1.38	2.29
Lower bearing	Top	2.72	4.65
	Middle	3.04	3.97
	Bottom	3.03	2.80

3.2 Effects of the annular depression on the shaft dynamic motion

To form the annular depression on the shaft surface is thought to affect not only the shaft supporting but also the shaft dynamic motion. Changes in the shaft motion at the crank pin induce the changes in the refrigerant gas leakage between the cylinder and piston. Therefore, effects of the annular depression on the shaft motion at the crank pin were investigated.

The displacements of the shaft center point at the middle of the crank pin $u_{Sic}(\theta)$, $v_{Sic}(\theta)$ were detected at all rotation angle under heating half-capacity operation and were plotted on Figure 5. $u_{Sic}(\theta)$, $v_{Sic}(\theta)$ is x- and y-directional displacement at the rotation angle θ, respectively. In Figure 5, the center and the radius of the circle represent the center of the bearing and the average clearance between the cylinder and piston. White circles and black circles represent the displacements obtained by the analysis of the normal shaft and the annular-depression-formed shaft, respectively. Index of each symbol represents the shaft rotation angle (degree). As shown in Figure 5, the shaft

center point at the middle of the crank pin obtained by the analysis of the annular-depression-formed shaft moves more extensively compared with that obtained by the analysis of the normal shaft, as the shaft rotates. The annular-depression-formed shaft is supposed to more bend and tilt compared with the normal shaft during the operation.

The refrigerant gas leakage between the cylinder and piston is influenced by the minimum clearance between the cylinder and piston $\delta_{cp}(\theta)$ (Ishii et al., 2008).

When the clearance between the crank pin and piston is assumed to be constant during the rotation, $\delta_{cp}(\theta)$ can be estimated based on $u_{Sic}(\theta)$, $v_{Sic}(\theta)$ plotted on Figure 5. As shown in Figure 5, $\delta_{cp}(\theta)$ changes according to the rotation angle θ. Therefore, the gas leakage correspondingly changes during the rotation.

Matsui et al. (2009) developed an analytical model coupling a dynamic mechanical analysis and refrigerant pressure analysis of a compressor combined with an expander, talking effects of gas leakage in consideration. Based on this analytical model, a volume efficiency of both compressors with the normal shaft and annular-depression-formed shaft was analyzed, talking the change in $\delta_{cp}(\theta)$ in consideration. As a result, the volume efficiency of the compressor with the annular-depression-formed shaft was increased by 0.3 % from that obtained by the normal shaft. This suggests that forming the annual depression on the shaft surface has a possibility to reduce the losses due to the refrigerant gas leakage and improve the volume efficiency.

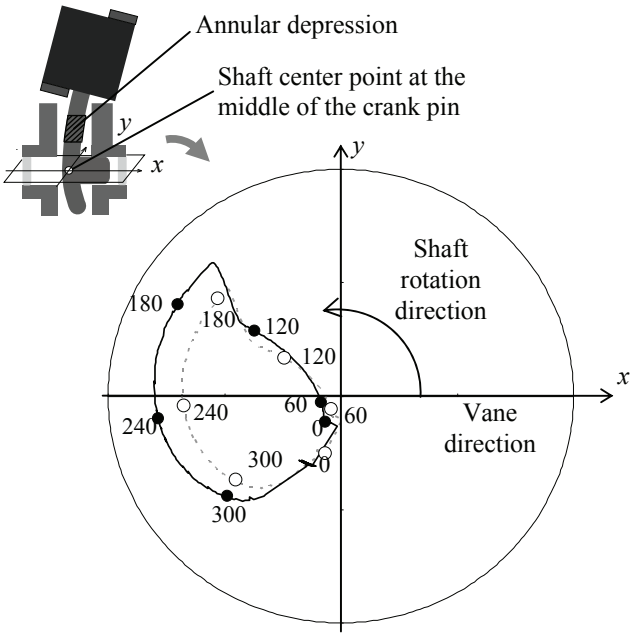

Figure 5: Shaft center point locus at the middle of the crank pin

3.3 Experimental results

Table 2 shows experimental results obtained by using the normal shaft and the annular-depression-formed shaft. The experiments were examined under heating half-capacity operation. After the experiment of the normal shaft, the annular depression of 200 μm was formed on the same shaft surface at the middle of the upper bearing and it was used for the experiment of the annular-depression-formed shaft. Except for the shaft, same experimental components were used in both experiments. As shown in Table 2, an energy supply for the compressor and volume efficiency were investigated. In Table 2, each resultant value was normalized by corresponding resultant value obtained by the experiment of the normal shaft.

As shown in Table 2, the energy supply and volume efficiency obtained by the experiment of the annular-depression-formed shaft was reduced by 0.4 % and increased by 0.2 % from those obtained by the experiment of the normal shaft, respectively. As a result, COP was improved by 0.6 %.

Although the analytical estimation of the increment of the volume efficiency was 0.3 %, the experimental result showed the increment of it by 0.2 %. This difference was caused by several assumptions made in the analytical model. At the analytical model, the change in the shaft dynamic motion due to the annular depression was assumed to affect the refrigerant gas leakage only between the cylinder and piston. However, the change in the shaft motion is thought to induce the change in the refrigerant gas leakage also between the piston top/bottom side and cylinder head. In addition, although it was assumed that the clearance between the piston and crank pin keeps constant during the operation, it is doubtful that this assumption meets the phenomenon. The clearance between there is not constant and is thought to have a distribution, like that between the shaft and bearing. This clearance distribution is possibly affected by the shaft dynamic motion.

Table 2: Experimental result under heating half-capacity operation

Shaft type / Experimental data	Energy supply	Volume efficiency
Normal shaft	1	1
Annular-depression-formed shaft	0.996	1.002

4. CONCLUSIONS

The elasto-hydrodynamic-lubrication taking the elastic deformation of both the bearing and shaft into consideration was developed. Obtained findings are as follows;
(1) The upper bearing hardly contributes to the shaft supporting in our compressor.
(2) The shaft center point at the middle of the crank pin of the annular-depression-formed shaft moves more extensively compared with that of the normal shaft during the operation, resulting in the shorten of the clearance between the piston and cylinder at some rotation angle. Therefore, to form the annular depression on the shaft surface reduces the losses due to the refrigerant gas leakage and increases the volume efficiency.
Based on above-mentioned finings, the annular depression was formed on the shaft surface at the middle of the upper bearing to improve the efficiency of the compressor. A consistency between analytical estimations and experimental results in the qualitative tendency of the loss reduction was confirmed. Experimental results showed that the annular-depression-formed shaft improved COP by 0.6 %.

NOMENCLATURE

p	oil film pressure	(Pa)
R	radius of the bearing	(m)
θ	shaft rotation angle	(m)
h	oil firm thickness at a local point	(m)
$\bar{h}_T$	expectation of h	(m)
η	lubricant oil viscosity	(Pa·s)
U	shaft rotation speed	(rad/s)
ϕx, ϕz, ϕs	collection factors for modified Reynolds equation	(-)
p_c	solid contact pressure	(Pa)
k'	factor of material and surface property of the two contact objects	(-)
E'	combined young's modulus of the shaft and bearing	(Pa)
σ	combined surface roughness of the shaft and bearing	(m)
$\delta_{cp}(\theta)$	minimum clearance between the cylinder and piston at the rotation angle θ	(m)
Fb_x	x-directional support force of the bearing	(N)
Fb_y	y-directional support force of the bearing	(N)
Fb_x^*	assumed-x-directional support force of the bearing	(N)
Fb_y^*	assumed-y-directional support force of the bearing	(N)
k_{xx}, k_{xy}, k_{yx}, k_{yy}	support force constants	(N/m)
$u_{Sic}(\theta)$	x-directional displacement of the shaft center point at the middle of the crank pin at the rotation angle θ	(m)
$v_{Sic}(\theta)$	y-directional displacement of the shaft center point at the middle of the crank pin at the rotation angle θ	(m)

REFERANCES

Patir, N., Cheng, H. S., 1978, Application of Average Flow Model for Determining Effects of Three-dimensional Roughness on Partial Hydrodynamic Lubrication, *Trans.ASME, Journal of Lubrication Technology*, vol. 100, No.1: p. 12-17.

Patir, N., Cheng, H. S., 1979, Application of Average Flow Model to Lubrication between Rough Sliding Surfaces, *Trans.ASME, Journal of Lubrication Technology*, vol. 101, No.4: p. 220-230.

Greenwood, J.A., Tripp, J. H., 1970, The contact of Two Nominally Flat Rough Surfaces, *Proceedings of the institution of mechanical engineers*, vol. 185, No.48: p. 625-633.

Patir, N., Cheng, H. S., 1978, Effect of Surface Roughness Orientation on the Central Film Thickness in E.H.D. Contacts, *Proceedings of the fifth Leeds–Lyon symposium on Tribology*: p. 15-21.

Ishii, N., Oku, T., Anami, K., Knisely, C. W., Sawai, K., Morimoto, T., Fujiuchi, K., 2008, Effects of Surface Roughness upon Gas Leakage Flow through Small Clearances in CO_2 Scroll Compressors, *International Compressor Engineering Conference at Purdue*, 1429.

Matsui, M., Hasegawa, H., Ogata, T., Wada, M., 2009, Development of the High-Efficiency Technology of a CO_2 Two-Stage Rotary Expander, *HVAC & R Research*, vol. 15, No. 4: p.743-758.